Yaroshenko, V., Miloch, W., Lühr, H. (2015): Particle-in-cell simulation of spacecraft/plasma interactions in the vicinity of Enceladus. - *Icarus*, *257*, p. 1-8.

DOI: http://doi.org/10.1016/j.icarus.2015.04.028

Particle-in-cell simulation of spacecraft/plasma interactions in the vicinity of Enceladus

V.V. Yaroshenko[a,*], W. J. Miloch[b], H. Lühr[a]

[a] *GFZ German Research Center For Geosciences, Telegrafenberg, 14473 Potsdam, Germany*
[b] *Department of Physics, University of Oslo, PB Box 1048 Blindern, N-0316 Oslo, Norway*

Abstract

The Cassini Langmuir Probe of the Radio and Plasma Wave Science instrument has measured an electron depletion in a region extending at least 50 satellite radii away from Saturn's small but geologically active icy moon Enceladus. The maximal imbalance between the electron and ion densities was observed in the dust loaded plume and to date is attributed to the electron attachment to abundant dust grains. We report the results from a three dimensional particle-in-cell simulation of a plasma structure formed around a charged spacecraft in the conditions relevant inside the Enceladus torus and in the moon's plume. In addition to the plasma population the plume simulation includes singly charged nanograins detected by the Cassini Plasma Spectrometer. The accompanied spacecraft plasma perturbations can significantly modify an ambient plasma at the Cassini Langmuir probe positions and thus impact the plasma measurements. Our modeling reveals a domination of water group ions over the electron population due to the formation of a conventional plasma sheath at the ram-oriented probe positions in the Enceladus torus and in the plume regions with low dust density ($n_{d0} < n_{e0}$). In the dust-dominated plume ($n_{d0} > n_{e0}$) the plasma perturbations are strongly reduced in the ram direction but can significantly compromise the probe measurements in the orbiter wake. Simulation results can qualitatively explain the long profiles of the electron-ion imbalance

*V. V. Yaroshenko

Email addresses: yarosh@gfz/potsdam.de (V.V. Yaroshenko), w.j.miloch@fys.uio.no (W. J. Miloch), hluehr@gfz/potsdam.de (H. Lühr)

registered by the Cassini Langmuir probe during the flybys E2, E3 and E5. In either case, the plasma perturbations associated with the moving Cassini orbiter appear to be important for reliable interpretations of the Langmuir probe measurements.

Keywords: `Saturn, Enceladus, Plume, Cassini, Plasma, Dust, Spacecraft potential, Wake.`

1. Introduction

The geologically active small moon Enceladus (radius $R_E \simeq 252$ km) represents a significant source of gas from geysers located at the moon's southern pole (*Porco et al.*, 2006). It is assumed that the plumes of gas that extend at least several R_E into space produce a radially narrow $\sim 1 R_S$ (Saturn radius $R_S = 60268$ km) torus of water-group neutral atoms and molecules centered on Enceladus' orbit (*Johnson et al.*, 2005). The main constituents of a weakly ionized plasma in the moon's torus are co-rotating water group ions and thermal electrons.

Another plasma occurs in the direct vicinity of the eruptive south pole of Enceladus. The plumes of neutral water-vapor interact directly with Saturn's co-rotating plasma, loading the magnetosphere with fresh cold ions and decelerating the co-rotating plasma flow up to its stagnation (*Tokar et al.*, 2006). The Enceladus plumes also contain copious amounts of charged dust. The micron-sized dust was detected by the Cassini Cosmic Dust Analyzer (CDA) instrument (*Spahn et al.*, 2006) and is visible in the forward scattering sunlight images from the Cassini Ultraviolet Imaging Spectrometer (*Porco et al.*, 2006). The smallest, nanometer-sized, icy grains have been registered by the Cassini Plasma Spectrometer (CAPS) (*Jones et al.*, 2009). Hill et al., 2012 reported the number densities up to $\sim 10^3$ cm^{-3} for negatively charged nanograins observed by CAPS at the close moon flybys. Numerous icy grains emanating from the moon interior and charged by an ambient plasma form together with thermal electrons and ions a dust-loaded plasma which is associated with the term

"plume". In the direct proximity to the moon's orbit, we thus can distinguish two different plasmas: a co-rotating electron-ion plasma of the Enceladus torus and a dust-loaded plasma of the plume with an almost stagnated plasma flow.

The Cassini spacecraft (SC) has made several targeted Enceladus flybys. The passages E3 (12 Mar 2008), and E5 (9 Oct 2008) are of specific interest since Cassini traversed a continuously changing plasma from the Enceladus torus to the dust-loaded plume and most instruments were favorably oriented to study variations in the plasma parameters. Since the SC charging process and the wake formation depend on the local plasma characteristics, the electrostatic configuration around the orbiter inevitably exhibits these changes. Indeed, the previous studies show that the SC in Saturn's magnetosphere achieves its equilibrium potential and forms a stable potential configuration during a few ion plasma periods, ω_{pi}^{-1} (*Yaroshenko et al.*, 2011). In the near-Enceladus environment, this process typically develops at time scale $\sim 10^{-3}$ s which is much shorter than the Cassini passage time through the moon's plume $\sim 10^{2}$ s. The orbiter hence adjusts almost instantaneously to the equilibrium potential following changes in the local plasma parameters. A SC electrostatic configuration governs self-consistently the plasma particle distributions around the orbiter. In this study we present simulations of such a plasma structure when the orbiter passes two characteristic regions within the Enceladus proximity: (A) the Enceladus torus (far away from the south-pole plume); (B) the dust-loaded plume. To this end we calculate a self-consistent spatial plasma-wake distributions around a spherical SC model employing a three-dimensional particle-in-cell DiP3D code (*Miloch et al.*, 2009; *Miloch*, 2010). Previously, the SC-plasma configurations in Saturn's magnetosphere have been studied under the assumption that either all plasma species co-rotate with the planetary magnetic field (*Olson et al.*, 2011; *Yaroshenko et al.*, 2011), or involve cold, new-born water group ions (*Yaroshenko et al.*, 2012). Our present simulations now are mostly focused on the specific features of the near Enceladus environment relevant for the Cassini plume flybys E3 and E5, and include an effect of the charged dust species. The main goal of these numerical studies is to highlight significant differences

in the plasma-wake configurations formed around SC in the Enceladus torus and in the plume plasmas, and to examine how they could help to explain the Cassini Langmuir Probe (LP) of the Radio and Plasma Wave Science (RPWS) instrument data obtained during the E3 and E5 flybys.

2. Model and numerical code

CAPS, RPWS instrument and Cassini magnetometer data have been used to constrain the parameter space for the modeling of the SC-plasma interactions. Here we consider the cumulative effect of the water group ions, introducing their average mass $m_i = 18$ amu. In the Enceladus frame of reference the rigid co-rotation speed is $V_{cor} \sim 26.4$ km/s. CAPS data however indicate an sub-corotating ion flow velocities ($\sim$80% of co-rotation) in the vicinity of the moon orbit (*Wilson et al.*, 2009). Measurements of the upper hybrid resonance frequency by the RPWS instrument provide estimates of the electron density in the range $n_{e0} \sim (45, 70)$ cm^{-3} at the moon's orbit (Gurnett et al. 2004). It is reasonable to identify these estimates with a total plasma density n_0 in the Enceladus torus. The CAPS observations during a few equatorial flybys of 2005 through the moon's torus, yielded the core electron and ion temperatures $T_e \in (1, 2)$ eV , $T_i \in (20, 30)$ eV, respectively (*Tokar et al.*, 2008, 2009).

In the plume plasma interpretations of the LP measurements predict a local strong enhancement of the ion density up to $n_{i0} \sim 3 \times 10^4$ cm^{-3} (*Morooka et al.*, 2011; *Shafiq et al.*, 2011). It was assumed that some of ions can be trapped withing the sheaths of the sub-micron and micron-sized dust particles *Wahlund et al.* (2009). In any case, the reported high ion densities are not consistent with free ion population inferred from the magnetic field perturbations measured by Cassini during the available Enceladus flybys (*Kriegel et al.* (2011, 2014)). Moreover, recent studies of the RPWS data obtained during a few plume crossings indicate a rather weak local increase of the electron density up to $n_{e0} \sim 10^2$ cm^{-3} (*Ye et al.*, 2012). In our modeling the plasma number density is associated with the ion density (as it would be in the absence of neg-

Table 1: Input parameters of the simulations

Region	n_{i0} (cm^{-3})	T_i (eV)	V_i (km/s)	n_{e0} (cm^{-3})	T_e (eV)	n_{d0} (cm^{-3})	T_d (eV)	V_d (km/s)	$n_{i0} - n_{e0}$ (cm^{-3})
(A)	60	30	28	60	1	-	-	-	0
(B1)	10^2	3	14.4	90	1	10	0.03	14.4	10
(B2)	10^3	3	14.4	240	1	760	0.03	14.4	760

atively charged dust) and we adopt for the plume region values, $n_0 = n_{i0} \sim 10^2$-10^3 cm^{-3}, matching well the Cassini magnetic data (*Kriegel et al.* (2011, 2014)). Admitting a production of the water-group ions from the cold plume neutral exosphere, we assume the ion temperature to be of $T_i \sim$3 eV. Note that the latter quantity is not constrained by Cassini observations, but is close to the predictions of the plume modeling by (*Fleshman et al.*, 2010). Furthermore, we introduce a new plasma species - nanometer-sized dust grains - as negatively singly charged ($q_d/e \sim 1$) heavy ions with mass/charge ratio $\sim 10^3$ amu/e. The nanograin densities, n_{d0}, registered by the CAPS instrument varied in a range $\sim$ 1-10^3 cm^{-3} deeply inside the plume (*Hill et al.*, 2012). Incorporating charged dust, we consider two plume cases. The first one (B1) describes a more rarefied plasma with $n_0 = n_{i0} \sim 10^2$ cm^{-3} and $n_{d0} \sim 10$ cm^{-3}. As we will see later, even such small amount of dust particles enables significant modifications of the plasma structure around the orbiter. The second case, B2, accounts for the densest part of the plume where the plasma density is assumed to be constrained by the measurements of the Cassini magnetometer, i.e. $n_0 = n_{i0} \sim 10^3$ cm^{-3} (*Kriegel et al.* (2011, 2014)). Simultaneously, we consider the high dust density $n_{d0} \sim 760$ cm^{-3} close to values registered by CAPS (*Hill et al.*, 2012). In both B1 and B2 cases, the plume dust particles are assumed to be cold with temperatures close to the neutral gas and we assign $T_d \sim 0.03$ eV. Table 1 summarizes the input average plasma parameters adopted in the PIC simulations for the regions of the Enceladus torus (A) and plume (B).

The difference between A and B plasmas includes not only variations in the plasma parameters and composition, but also modifications of the "geometry" of SC-plasma interactions. To clarify the geometrical aspect we consider the plume flyby E3 which took place on 12 March 2008 with the closest approach to Enceladus of ∼50 km. The projection of the Cassini E3 trajectory onto the XZ plane of the coordinate system associated with the moon is shown in Fig. 1. Here we use a so called Enceladus Interaction Coordinate System (ENIS), co-rotating with Saturn. Its Z-axis is aligned with the moon's rotation axis, pointing roughly toward ecliptic north. The Y-axis points toward Saturn. Then the X-axis completes the right handed coordinate system in the direction of motion of Enceladus around Saturn. The two panels in Fig.1 illustrate the difference between the plasma regions A and B. The left one shows a part of the Cassini trajectory, when the orbiter is at large distances $\geq 40R_E$ from the moon and when the ion flow, being unaffected by the plume products, is in the azimuthal direction. Since the co-rotating ion flow and the SC velocity vector constitute an angle $\geq \pi/2$, this ensures a high relative SC-ion velocity $|\mathbf{V}_i| = |\mathbf{V}_{cor} - \mathbf{V}_{SC}| \sim 30$ km/s. In our simulations for the case A we assign $V_i \simeq$28 km/s. The latter quantity matches the ion flow velocity at 18:51 UT (12 March, 2008), if the ideal co-rotation velocity is reduced to $V_{cor} \sim 23$ km/s. As Cassini approached the moon's plume (right panel in Fig. 1), the neutral water-vapor reacts with Saturn's co-rotating plasma, loading the magnetosphere with fresh cold ions with subsequent slowing of the co-rotating flow to its stagnation (*Tokar et al.*, 2006). In a central part of the plume we hence assume $\mathbf{V}_{cor} \to 0$, so that the relative ion velocity becomes $\mathbf{V}_i \simeq -\mathbf{V}_{SC}$. Admitting that the plume dust is initially coupled to the neutral gas yields the same relative velocity for the grains, i.e. $\mathbf{V}_d \simeq \mathbf{V}_i \simeq -\mathbf{V}_{SC}$. For the SC velocity in the plume (case B) we take $V_{SC} \simeq$14.4 km/s close to the Cassini speed at 19:07 UT.

At this stage it is convenient to introduce a local coordinate system (x, y) related to the moving orbiter where a relative plasma flow velocity, $\mathbf{V}_i$, determines the positive x direction. Both panels of Fig.1 show schematically such a coordinate system (x, y) , as it would look like if the SC moved only in the

XZ-plane of EICS. Note, that in a real situation the x-axis is directed along a three dimensional vector of the ion flow velocity $\mathbf{V}_i$ in the SC frame of reference so that only scalar velocities are involved in our simulation.

To study spatial plasma structures around the moving SC we employ a three dimensional particle-in-cell DiP3D simulation code, which calculates a self-consistent potential on an object and wake formation in the electrostatic approximation in intricate plasma environments. More details about this code are given elsewhere (*Miloch et al.*, 2009; *Miloch*, 2010) and here we present only the basics of the numerical modeling. In the particle-in-cell (PIC) method the plasma particles interact with each other via a computational grid that is used to calculate the force field. This reduces the complexity of calculations and makes the large-scale plasma simulations feasible. DiP3D is an electrostatic PIC code that operates in Cartesian coordinates and uses a regular grid. Its main computational cycle is standard (*Birdsall and Langdon* (2009)), and consists of weighting numerical particles to the nearest grid points, solving the Poisson equation and finding forces on the grid, projecting forces to the particles, and advancing particle trajectories. Trajectories of simulated particles are advanced with the leap-frog method (*Birdsall and Langdon* (2009)), which is characterized by a shifted time-mesh for velocities:

$$\begin{aligned} \vec{x}_i(t+\Delta t) &= \vec{x}_i(t) + \vec{v}_i(t+\Delta t/2)\Delta t \\ \vec{v}_i(t+\Delta t/2) &= \vec{v}_i(t-\Delta t/2) + \vec{f}_i(t)\Delta t/m_i \end{aligned} \tag{1}$$

where i refers to a simulated particle, $\vec{f}_i = q_i\vec{E}$ is an electric force projected on the i-th particle from the nearest grid points, and Δt is the computational time step. For solving the Poisson equation, a multigrid method is used (*Press et al.* (2009)).

The boundaries of the simulation box are open for simulated particles, and the particles can leave the box during simulation. At each time step the particles are also introduced through the boundaries according to fluxes accounting for relevant velocity distributions. Thus, the number of particles in the system is not fixed, but since the number of simulated particles is usually more than

10^7, quasineutrality at large scales is well maintained. DiP3D can simulate multispecies plasmas, with each of the species having a different drift velocity.

Spherically shaped objects can be introduced into the system, far away from the boundaries. The objects are charged self-consistently by plasma currents throughout the simulation. In addition, charging by photoemission due to unidirectional light can be included. DiP3D can simulate perfectly insulating and perfectly conducting objects. For insulators the charge of the particles that hit the surface remain at the object's surface in the hitting position and contribute to the local electric field at all later times. For conducting objects, the charge is redistributed on the surface as to cancel internal electric fields. In both cases, the objects act as sinks for the simulated particles.

The validity of the DiP3D code for Saturn's magnetosphere and for the dense Enceladus torus has been discussed by (*Yaroshenko et al.*, 2011, 2012). We use the same numerical procedure and approximations. In particular, our simulations do not include the effect of the planetary magnetic field except through the variations of the plasma flow: in the Enceladus torus the plasma ions are assumed to be frozen in Saturn's magnetic field and co-rotated with the planet (region A); in the plume region B, on the contrary, due to the magnetic field line draping and the mass loading the ion flow is slowed-down up to stagnation. Plasma particle gyration in Saturn's magnetic field is also not taken into account since their Larmor radii are much larger than the Cassini dimensions (e. g. the smallest electron gyro radius is of the order of 14 m). Following the analogy with the probe theory, we assume that in such a case the planetary magnetic filed does not significantly affect the SC charging process (see e.g.*Demidov et al.* (2002) and references therein). Moreover, based on results of *Yaroshenko et al.* (2011, 2014) we can neglect photo-emission and contribution of the photo-electrons to the SC charging in the direct vicinity of the moon. Finally, our studies employ a spherical model of the SC. Such an idealization is justified at distances larger than the plasma Debye length: in this case the numerical analysis reveals only small discrepancies due to the shape of the object (*Miloch et al.* (2007)). On the other hand, this simplified representation

will also be valid, as a first approximation, for non-spherical objects at smaller distances. In other words, we expect that a simplified spherical model captures the main physical features and thus can provide insight into intricate process of SC/plasma interactions in the near-Enceladus plasmas. By modeling the SC as a spherical conducting object of $\sim$ 6.6 m diameter, we adapt the code to include a new heavy plasma species - charged nanograins. The dust contribution is twofold. First, the charged grains can produce additional dust-associated currents and thus affect the equilibrium SC charge and the plasma configuration around the orbiter. On the other hand, negatively charged dust initially reduces the electron population ($n_{e0} = n_{i0} - n_{d0}$). To compare the plasma-wake configurations formed around the orbiter in the almost dust-free Enceladus torus (case A) and inside the dust-loaded plume (cases B1 and B2) we have simulated the SC/plasma interactions for the three sets of parameters given in Table 1.

3. Results

Figures 2 shows the contour plots of self-consistent potential and plasma distributions surrounding the orbiter in the A and B regions. All plots are given in the xy plane, cutting through the center of the spacecraft. In the considered cases, the plasma electrons are mainly responsible for the plasma screening (*Yaroshenko et al.* (2011)) and thus length scales in Fig.2 are measured in units of the electron Debye length, defined through $\lambda_D = (4\pi e^2 n_{e0}/m_e)^{1/2}$. The upper contour plots illustrate the case A, when the SC traverses the almost co-rotating plasma of the Enceladus torus and forms a wake-like structure downstream of the orbiter. The SC potential is of the order of $\psi_{SC} \sim -3$ V, however for presentation purposes, only small potential variations ($\psi \in (-0.5, 0)$ V) are colored in Fig. 2(A). While around an immobile spherical object embedded in a plasma the sheath potential drops equally in all directions due to a spherically symmetric distribution of the net space charge, the plasma flow around a charged SC produces a wake asymmetry in both, potential and plasma configuration downstream of the orbiter. Indeed, in case A the most of the potential

drop occurs on length scales of $\sim 5\lambda_D$ (downstream) and $\sim 3\lambda_D$ (upstream) in the white area. Cold electrons with thermal energy $T_e \sim 1$ eV$< e\,|\psi|$ cannot overcome the negative potential around the orbiter directly, and the resulting electron distribution is also asymmetric with similar scales $\sim 5\lambda_D$(downstream) and $\sim 3\lambda_D$ (upstream). Contrary to the electrons, the water group ions do not reveal significant density perturbations in the upstream direction, and form only a pronounced wake of $\sim 3\lambda_D$ downstream of the orbiter (upper right panel). There is no sign of an ion focusing effect: the ion kinetic energy $K_i \sim 80$ eV in the Cassini frame prevails over the thermal energy $T_i \sim 30$ eV and significantly exceeds the SC electrostatic potential $e\,|\psi_{SC}| \sim 3$ eV. On the other hand, due to high ion thermal energy ($T_i \sim 30$ eV) the ions can effectively fill the negative potential well downstream of the orbiter. Such a plasma configuration is in good agreement with typical potential distributions found for Cassini during Saturn orbit insertion flyby in the inner magnetosphere (Figs. 2-5 in *Yaroshenko et al.* (2011)).

The presence of dust grains in the plume modifies the potential and plasma configurations as shown in the lower plots of Fig.2. Introducing even a diluted grain population ($\sim$ 10 % of the plasma density), we found a much more pronounced spatial distribution of the potential $\psi\,(x,y)$, and plasma species, $n_e\,(x,y)$ and $n_i\,(x,y)$, downstream of the orbiter, which is charged to a lower potential, $\psi_{SC} \sim -4$ V. In the downstream region there is a clear sign of the extended ($\geq 20\lambda_D$) Mach cone in a potential structure $\psi\,(x,y)$ and associated with this a n_e- depletion region with a weak electron focusing far downstream from the orbiter surface, ($x \sim 25\lambda_D$). Another negative plasma component - the cold dust grains with a high kinetic energy $K_d \geq 1$ keV$\gg T_d$ (K_d in the SC frame of reference) displays a conventional geometric wake in the downstream region (similar to that shown in the lowest panel of Fig.2). The ions being not so energetic and much warmer than grains ($K_i \sim 20$ eV $> T_i \sim 3$ eV) form a kind of dispersed wake structure. The ion wake boundaries are not well defined and the wake scale, transverse to the plasma flow - along the y axis, becomes even larger than the SC size, similar to the enhanced wake

discussed by *Yaroshenko et al.* (2011). Comparative analysis of the A and B1 ion structures of Fig. 2 shows that a relation between the actual ion wake length and the plasma parameters is not straightforward. On the one hand, increase of the ion temperatures (as outside the plume) allows the ions to diffuse into the wake more efficiently and thus it shortens the wake structure. We see this effect when comparing the wake lengths in the cool plume (case B1) with the case of warm ions in the Enceladus torus (case A). On the other hand, the growth of the relative plasma flow in case A causes the wake to lengthen. It seems, however, that for the parameter regime relevant in the near-Enceladus plasmas the temperature effect dominates.

Continuing with the denser dust-loaded case (B2) and accounting for the additional dust-associated impacts, yields a less negative Cassini potential ($\psi_{SC} \sim -3$ V). Nevertheless, Fig.2 illustrates an even more extended and inhomogeneous plasma and potential configuration around the charged SC than the case B1. While the main carriers of negative charge - dust grains - form a geometric wake similar to the case B1 (lowest panel in Fig.2), the electron depletion around the orbiter becomes more widespread. It occurs now not only in the direct vicinity of the orbiter but predominantly along and adjacent to the grain's Mach cones. In contrast to the rarefied case B1, one finds a strong local electron density enhancement (by a factor of 2-3) directly in the vicinity of the SC, at distances $\geq 3\lambda_D$ downstream. Moreover, the ions do not form a dispersed wake structure as in B1 case, but reveal a rather typical extended wake configuration with the density reduction downstream and weakly depopulated Mach cones. The self-consistent potential perturbations demonstrate the well pronounced Mach cone structure with scale sizes of $\geq 30\lambda_D$ and display a slow growth of the electric potential deeply in the wake (up to $\psi \sim +1$ V). Such a configuration engenders an electron accumulation and ion depopulation within the wake as discussed above.

As seen, the plume conditions B2 give rise to a totally different plasma structure around the orbiter. This presumably originates from a combination of two tendencies. On the one hand, decrease in the electron Debye length

in the regime B2 (compared to A and B1) means that the orbiter has to be more strongly shielded. This engenders electron depletion much more closely to the SC surface and extends the quasineutral plasma region up to the distances $\sim 2.5\lambda_D \sim 1$ m in the upstream direction. On the other hand, both dominating species - the positive ions and negative heavy dust grains - form narrow elongated wakes downstream. Interplay between the two structural features results in the inhomogeneous potential configuration which self-consistently redistributes the plasma species providing the observed spatial picture in Fig.2(B2).

The most important consequence of our modeling is that the resulting plasma structure around the SC can be *a priori* significantly modified at the points characteristic for positions of the Cassini LP, and thus a probe mounted on the orbiter most likely cannot accurately measure an ambient plasma. The Langmuir probe is attached to Cassini on a 1.5 m deployable boom (*Gurnett et al.*, 2004), and in Figure 3 we give the angular distributions of the plasma imbalance $\delta n = (n_i - n_e)$ calculated at 1.5 m from the SC spherical surface in the xy plane for A, B1 and B2 cases shown in Fig.2. The angle θ counts from the positive x-direction so that $\theta = 0$ points to the wake center. Figure 3 indicates a similar dependence of $\delta n(\theta)$ in both plasmas - in the Enceladus torus and inside the plume. As seen, an instrument mounted at a 1.5 m-boom on the spherical model of the orbiter and oriented inside the wake ($\theta \simeq 0$) would register only a small misfit $\delta n/n_0 \leq 10\%$ in A and B1 plasmas. Such discrepancies are at the upper limit of the accuracy of the LP measurements (*Wahlund et al.*, 2009) and thus can hardly be reliably resolved. On the contrary, in the ram ($\theta \sim \pi$) direction the instrument would see a significant imbalance between the electron and ion densities **in both A and B1 cases**. In the moon's torus this effect is solely a manifestation of the inhomogeneous plasma sheath structure at the orbiter surface disturbed by the presence of the plasma flow, as discussed above. In accordance with Fig.3 the electron depletion in case A could reach $\delta n/n_0 \sim 60 - 65\%$ at the upstream direction. An even stronger imbalance up to $\delta n/n_0 \sim 70 - 75\%$ at $\theta \sim \pi$ in the moon's plume caused by the simultaneous action of two factors - the formation of a SC sheath structure and the

presence of negatively charged dust, which decreases the initial electron density and self-consistently modifies a space plasma distributions around the SC (see e.g. Fig. 2, case B1). It is important to stress that in our simulation of the plume case B1 the electron depletion is mainly caused by a spatial plasma distribution around the charged SC and to lower degree is imposed by the presence of a small fraction (n_d/n_0 ∼0.1) of negatively charged dust. Although at first glance a further growth of the dust number density seems to enhance the net imbalance δn in the upstream region, a high dust population can significantly alter a spatial plasma structure around the SC. Indeed as found in the dust-dominated case B2, the initial electron depletion $(n_{i0} - n_{e0})/n_0 \sim 76\%$ is not strongly modified at the ram-oriented LP positions (see Fig.3, right panel). A maximal net electron depletion $\delta n/n_0 \simeq 85\%$ is achieved at a LP position $\theta \sim 100^\circ$ and with further growth of θ the plasma imbalance reduces to the almost ambient plasma value $\sim 76\%$. Consequently, the electron depletion in the ram direction mainly reflects the existence of numerous negatively charged dust particles initially accumulating the plasma electrons. The LP measurements in the ram direction will thus be weakly subject to the plasma perturbations in agreement with plasma distributions shown in Fig.2 (B2). In contrast to the ram direction, the wake-orientated LP will sense an almost quasineutral plasma ($\delta n/n_0 \simeq 2 - 4\%$) instead of the realistic value $\delta n/n_0 \simeq 76\%$.

The Cassini LP/RPWS measurements made during Enceladus flybys E3 and E5 suggest that the electron density is less than the ion density already at large distances from the moon achieving $n_i \gg n_e$ in the dust loaded plume (Fig. 5, in (*Morooka et al.*, 2011)). The electron depletion has been solely attributed to the electron attachment to the abundant sub-micron-sized dust particles (*Yaroshenko et al.*, 2009; *Farrell et al.*, 2009, 2010; *Shafiq et al.*, 2011). In the light of the results shown in Fig. 3, however, the measured electron depletion could be a manifestation of the plasma structure formed around the moving orbiter. Indeed, during both flybys, E3 and E5, LP registered a strong plasma imbalance extended far away from the moon with the maximum $\delta n/n_0 \simeq 95\%$ in the central part of the Enceladus plume (19:06:45 UT for E3 and ∼19:07

UT for E5, respectively) (*Morooka et al.*, 2011; *Shafiq et al.*, 2011). During the plume traversing the probe was oriented at angles $\beta \sim 27^\circ$ (E3) and $\beta \sim 23^\circ$ (E5) with respect to the SC velocity. Using the Cassini ephemeris database (http://www-pw.physics.uiowa.edu/ jbg/cas.html) around ∼19:06:45 UT (E3) and 19:07 UT (E5) and keeping the azimuthal ion flow velocity (V_{cor}) as a free parameter we have retrieved the reference angle θ involved in our modeling. It turns out that an assumption on slow plume ions ($V_{cor} \in (0, 2)$ km/s) gives the narrow window for angles $\theta \in (150^\circ, 160^\circ)$ for both plume passes. Such upstream LP positions in the plume, according to Fig. 3, immediately provide the maximal plasma imbalance $\delta n/n_0 \sim 70\% - 75\%$. It seems quite reasonable to assume that this effect is most likely due to the presence of the numerous negative grains in the dust-dominated part of the plume ($n_{d0} > n_{e0}$, B2 case). Outside the densest plume region ($n_{d0} < n_{e0}$, B1 case) δn is rather a manifestation of inhomogeneous plasma structure at the LP position. Prior to and after the plume passage the LP orientation angle β was slowly increased during both flybys. Moreover, the azimuthal co-rotating flow comes into play significantly increasing the relative ion flow velocity V_i. These factors decrease the angle θ with distance from the plume. For example, assuming a full co-rotating flow far away from the plume yields the angle $\theta \sim 45^\circ$ at distance $Z \sim 115R_E$ (at 18:30 UT) and $\theta \sim 70^\circ$ at distance $Z \sim -77R_E$ (at 19:30 UT). In accordance with curves A and B1 in Fig.3, such a decreased θ could provide a consequent reduction in the plasma imbalance to $\delta n/n_0 \sim 25\% - 30\%$ and $\delta n/n_0 \sim 50\%$, respectively. The latter tendency is fully consistent with the Cassini LP measurements during E3 flyby: weak misfits of the plasma densities $\delta n/n_0 \leq 20\%$ before ($Z \sim 50R_E$) and after ($Z \sim 80R_E$) the plume encounter, and a significant increase $(n_i - n_e)/n_0 \sim 95\%$ in the dust loaded plume (see Fig. 4 in (*Morooka et al.*, 2011)). As we have checked, similar conclusions are also valid for the E5 flyby (9 Oct. 2008) for which the maximal density imbalance $\delta n/n_0$ occurs at the central part of the plume, when the LP looks in the upstream direction ($\theta \sim 140^\circ - 160^\circ$ at 19:07 UT), while far from the plume the angle θ decreases (e.g. $\theta \sim 80^\circ - 90^\circ$ at 19:30 UT and $Z \sim -90R_E$) with a consequent drop of

$\delta n/n_0$.

Our simulations show that a radial dependence of the plasma imbalance, δn, recorded by the Cassini LP/RPWS might be at least partially, if not dominantly, a result of the inhomogeneous plasma structure formed around the SC. Indeed, the electron depletion δn can reach significant values providing ratios $n_e/n_i \sim 0.3 - 0.25$ without invoking negatively charged dust at possible LP/RPWS positions.

Before closing this section, it is worth speculating about possible application of our results to the Enceladus flyby E2 (14 July, 2005), when for the first time the Cassini LP detected a significant electron depletion in the vicinity of the moon (*Yaroshenko et al.*, 2009; *Wahlund et al.*, 2009). The LP registered $n_e \neq n_i$ between $\sim$ 19:44 - 20:02 UT with a maximum plasma imbalance at $\sim$ 19:55 UT. Following the same outline, we examine whether the proper LP orientation corresponds to the maximum of the observed plasma imbalance δn. In contrast to the E3 and E5 flybys, this encounter occurred upstream of the moon, and the SC did not pass through the dust-loaded plume. The main difficulty in the application of our models to the E2 passage is that the ion flow velocity has been significantly slowed and deflected over a large volume extended more than the region where the electron depletion has been observed (see Fig. 4 in *Tokar et al. 2006*). In other words, this flyby does not corresponds to the discussed geometry of Fig.1. The uncertainties in the plasma flow velocity might produce a wide range of possible angles θ, and this hinders a determination of a single value of the electron depletion at a certain point of the E2 trajectory. So only some qualitative conclusions resulting from Fig.3 can be made. Assuming that the co-rotating velocity is deflected by an angle α (counting from the azimuthal direction within Saturn's equatorial plane, positive from Saturn) we show in Fig. 4 the angle θ as a function of the deflection angle α at reduced flow velocities $V_{cor} \leq 20$ km/s. In the calculations we have used the Cassini ephemeris and LP coordinates at $\sim$ 19:55 UT. As seen, small flow deflections ($\alpha \leq 30^\circ$), ultimately lead to the upstream LP positions with typical $\theta \sim 125^\circ - 175^\circ$. Based on our results shown in Fig.3 (left panel) we anticipate a maximal plasma imbalance

$\delta n/n_0 \sim 60-70\%$ mainly due to the SC sheath structure. Interestingly enough, these numbers give an electron depletion close to those observed by the Cassini LP (Fig. 1 by *Yaroshenko et al.* (2009) gives $(\delta n/n_0)_{max} \sim 65\%$). Assuming the ion flow velocity at $\sim$ 19:44 UT and $\sim$ 20:02 UT close to interpolations given in Fig.4 by *Tokar et al.* (2006) at $t = t_2$ and $t = t_4$, respectively, yields $\theta \leq 100^\circ$ and reduces the plasma imbalance to $\delta n/n_0 \leq 50\%$. As seen our results qualitatively match the E2 electron depletion data measured between $\sim$ 19:44 - 20:02 UT. The rather large uncertainty introduced by the ion flow variations in the direct vicinity of the moon cautions us to make exact quantitative comparisons with the E2 LP measurements.

4. Summary

We have presented results of PIC simulations that predict how a spherical model of the Cassini SC interacts with (A) the co-rotational plasma flow in the Enceladus torus and (B) the stagnated ion flow and dust grains in the plume. Our numerical analysis has two important consequences. First, it points out that plasma perturbations accompanying the charged SC are strongly dependent on the ambient plasma models, and even a small amount of negative dust ($n_d/n_0 \sim 0.1$) initiates a much more complicated plasma and potential distributions around the orbiter than those formed in the conventional electron-ion plasma (Fig.2). Second, the resulting plasma configurations can directly impact the ambient plasma density measurements by the Cassini LP. In the Enceladus torus and in the plume regions with the dust density obeying $n_{d0} < n_{e0}$ we found a significant domination of water group ions over the electron population in the ram direction due to the formation of a conventional plasma sheath. This leads to the electron depletion $n_e/n_i \sim 0.3 - 0.4$ at $\theta \sim \pi$ at distances $\sim$ 1.5 m from the SC surface (Fig.3, A and B1 cases). The latter implies that the ram-oriented LP will register a non-quasineutral plasma with $n_e/n_i < 1$ instead of $n_e \sim n_i$. In the dust-abundant plume with $n_{d0} > n_{e0}$ (B2 case) the negative dust provides an initial electron depletion (ambient plasma depletion) which re-

mains a main factor affecting the plasma and potential distributions around the orbiter. The associated plasma perturbations are strongly reduced at ram LP positions and the probe can make relatively accurate measurements of the ambient plasma. Contrary to the upstream situation, in the downstream direction the electron depletion at the LP positions decreases in all, A and B, plasmas and in the limit $\theta \sim 0$ it is reduced to $\delta n/n_0 \sim 0.1$ (A, B1) and $\delta n \sim 0.02$ (B2), respectively. Hence the wake-oriented LP will always sense $n_e \approx n_i$ which is relatively accurate for A and B1 plasmas, but gives significantly compromised measurements in the dust-dominated B2 case. Our findings therefore indicate that great care has to be taken by inclusion of the LP orientation and plasma models in the interpretations of the probe data. Moreover, the observed electron depletion cannot not be always attributed only to the electron attachment to the dust particles, as has been discussed in the previous studies (*Farrell et al.*, 2009, 2010; *Wahlund et al.*, 2009; *Yaroshenko et al.*, 2009; *Morooka et al.*, 2011; *Shafiq et al.*, 2011).

Finally, note that although our modeling can qualitatively explain the trend of some Cassini LP measurements with long intervals of the electron-ion misfit, extending far away from the dust-reached regions, the simulation results need to be systematically updated as more Cassini data on the near-Enceladus plasma become available.

5. Acknowledgment

This work has been supported by the Deutsche Forschungsgemeinschaft (DFG) under the grant YA 349/1-1 (Special Program, PlanetMag, SPP 1488). The authors thank Dr. Sean Hsu for helpful discussion of the Cassini LP data and unknown referees for the constructive comments on the manuscript.

References

C. K. Birdsall and A. B. Langdon, Plasma Physics via Computer Simulation (Adam Hilger, Bristol, 1991).

Demidov, V. I., S. V. Ratynskaia, and K. Rypdal (2002), Electric probes for plasmas: The link between theory and instrument, *Rev. Sci. Instrum., 73*, 34093440.

Farrell, W. M., et al. (2009), Electron density dropout near Enceladus in the context of water-vapor and water-ice, Geophys. Res. Lett., 36, L10203, doi:10.1029/2008GL037108.

W. M. Farrell, W. S. Kurth, R. L. Tokar, et al. 2010, Modification of the plasma in the near-vicinity of Enceladus by the enveloping dust. Geophys. Res. Lett. 37, L20202, doi:10.1029/2010GL044768, 2010

Fleshman, B. L., P. A. Delamere, and F. Bagenal (2010), A sensitivity study of the Enceladus torus, Geophys. Res. Lett, 37, L03202, doi:10.1029/2009GL041613.

D. A. Gurnett et al., 2004, The Cassini radio and plasma wave investigation. Space Sci. Rev. 114, 395-463.

Hill, T. W., M. F. Thomsen, R. L. Tokar, A. J. Coates, G. R. Lewis, D. T. Young, F. J. Crary, R. A. Baragiola, R. E. Johnson, Y. Dong, R. J. Wilson, G. H. Jones, J.-E. Wahlund, D. G. Mitchell, and M. Horányi, (2012) Charged nanograins in the Enceladus plume, *J. Geophys. Res., 117*, A05209.

Johnson, R. E., M. Liu, and E. C. Sittler Jr. (2005), Plasma-induced clearing and redistribution of material embedded in planetary magnetospheres, Geophys. Res. Lett., 32, L24201, doi:10.1029/2005GL024275.

Jones G.H. et al.(2009), Fine jet structure of electrically charged grains in. Enceladus' plume, *Geophys. Res. Lett. 36*, L16204.

Kriegel, H., S. Simon, U. Motschmann, J. Saur, F. M. Neubauer, A. M. Persoon, M. K. Dougherty, and D. A. Gurnett (2011), Influence of negatively charged plume grains on the structure of Enceladus Alfvn wings: Hybrid simulations versus Cassini magnetometer data, *J. Geophys. Res., 116*, A10223.

Kriegel, H., S. Simon, P. Meier, U. Motschmann, J. Saur, A. Wennmacher, D. F. Strobel, and, M. K. Dougherty, (2014), Ion densities and mag- netic signatures of dust pickup at Enceladus, *J. Geophys. Res., 119*, 27402774,

Miloch et Miloch, W. J., H. L. Pécseli, and J. Trulsen (2009), Numerical simulations of the charging of dust particles by contact with hot plasmas, *Nonlinear Processes Geophys. 14*, 575-586.

Miloch, W. J., S. V. Vladimirov, H. L. Pécseli, and J. Trulsen (2009), Charging of insulating and conducting dust grains by flowing plasma and photoemission, *New J. Phys., 11*, 043005.

Miloch, W. J. (2010), Wake effects and Mach cones behind objects, Plasma Phys. Controlled Fusion, 52, 124004.

Morooka, M. W., J.-E. Wahlund, A. I. Eriksson, W. M. Farrell, D. A. Gurnett, W. S. Kurth, A. M. Persoon, M. Shafiq, M. André, and M. K. G. Holmberg (2011), Dusty plasma in the vicinity of Enceladus, *J. Geophys. Res., 116*, A12221.

Olson, J., W. J. Miloch, S. Ratynskaya, and V. Yaroshenko (2010), Potential structure around the Cassini spacecraft near the orbit of Enceladus, Phys. Plasmas, 17, 102904.

Porco, C. C., et al. (2006), Cassini observes the active south pole of Enceladus, Science, 311, 1393 - 1401

W. H. Press et al., Numerical Recipes in C: The Art of Scientific Computing (Cambridge University Press, New York, 2002).

Shafiq, M., J.-E. Wahlund, M. W. Morooka, W. S. Kurth, and W. M. Farrell (2011), Characteristics of the dust-plasma interaction near Enceladus' south pole, *Planet. Space Sci.*, *59*, 17–25.

Spahn, F., et al. (2006), Cassini dust measurements at Enceladus and implications for the origin of the E ring, *Science, 311*, 1416–1418.

Tokar, R. L., R. E., Johnson, T. W. Hill, et al. , (2006), The interaction of the atmosphere of Enceladus with Saturn's Plasma, *Science*, *311*, 1409-1412.

Tokar, R. L., et al. (2008), Cassini detection of water-group pick-up ions in the Enceladus torus, *Geophys. Res. Lett., 35*, L14202.

Tokar, R. L. , R. E. Johnson, M. F. Thomsen, R. J. Wilson, et al. (2009), Cassini detection of Enceladus' cold water-group plume ionosphere *Geophys. Res. Lett.*, *36*, L13203.

Wahlund, J. E., et al. (2009), Detection of dusty plasma near the E-ring of Saturn, Planet. Space Sci., 57, 17951806.

R. J. Wilson, R. L. Tokar, and M. G. Henderson. Thermal ion flow in Saturn's inner magnetosphere measured by the Cassini plasma spectrometer: A signature of the Enceladus torus? Geophys. Res. Lett 36, L23104, doi:10.1029/2009GL040225

Yaroshenko, V. V., S. Ratynskaia, J. Olson, N. Brenning, J.-E. Wahlund, M. Morooka, W. S. Kurth, D. A. Gurnett, and G. E. Morfill (2009), Characteristics of charged dust inferred from the Cassini RPWS plasma measurements in the vicinity of Enceladus, Planet. Space Sci., 57, 18071812.

Yaroshenko, V. V., W. J. Miloch, S. Vladimirov, H. M. Thomas, and G. E. Morfill (2011), Modeling of Cassinis charging at Saturn orbit insertion flyby, J. Geophys. Res., 116, A12218, doi:10.1029/2011JA016775.

Yaroshenko, V. V., W. J. Miloch, H. M. Thomas, and G. E. Morfill (2012), Cassini capturing of freshly-produced water-group ions in the Enceladus torus, Geophys. Res. Lett, 39, L18108, doi:10.1029/2012GL053173.

Yaroshenko, V. V., H. Lühr and W. J. Miloch, (2014), Dust charging in the Enceladus torus, *J. Geophys. Res. Space Physics, 119,* 221236, doi:10.1002/2013JA019213.

Ye, S.-Y., D.A. Gurnett, W.S. Kurth, T.F. Averkamp, M. Morooka, S. Sakai, and J.-E. Wahlund, Electron Density Inside Enceladus Plume Inferred from Plasma Oscillations Excited by Dust Impacts, J. Geophys. Res., 119, pp. 3373-3380, doi:10.1002/2014JA019861

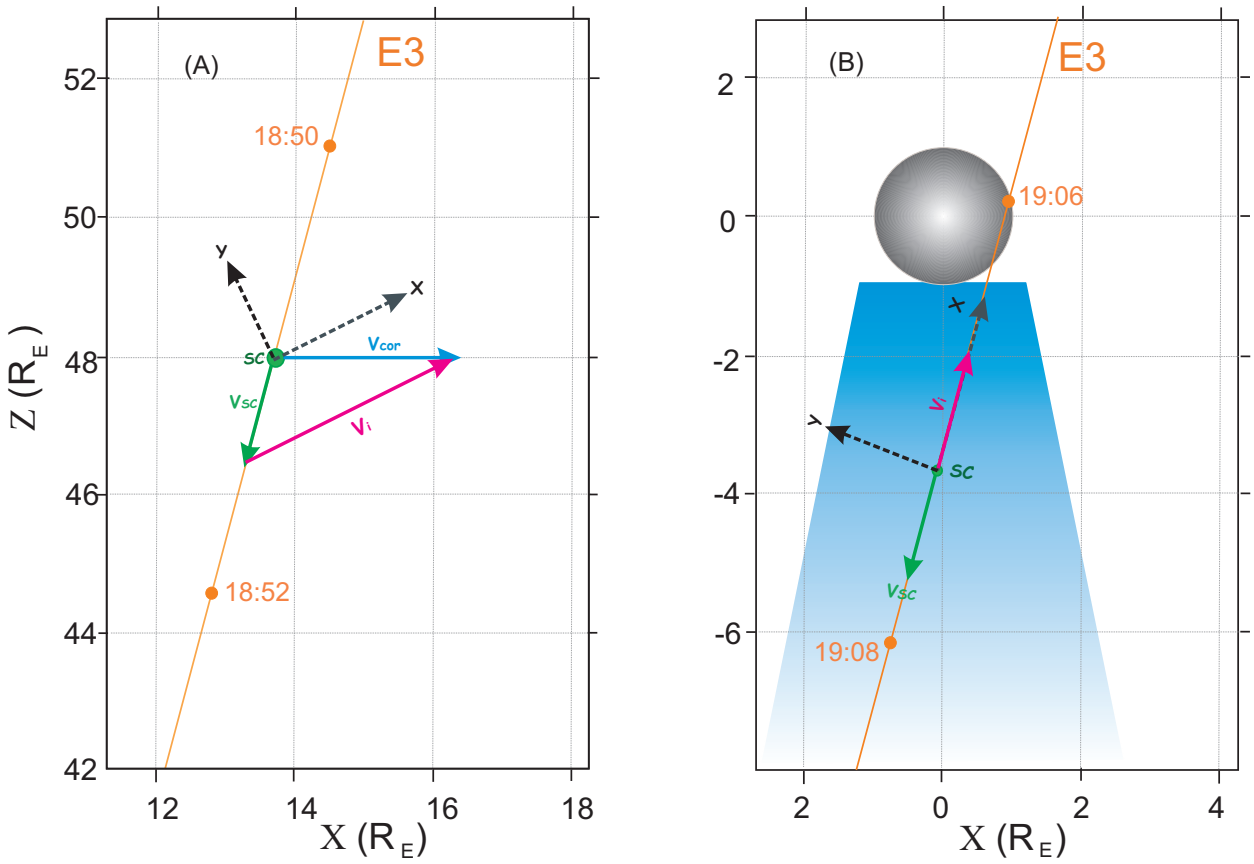

Figure 1: Cassini Flyby E3 in the XZ plane of the Enceladus Interaction Coordinate System (EICS) and local coordinate systems (x, y) used in simulation. Left panel illustrates case A, when Cassini is exposed to the co-rotating electron-ion plasma far away from the plume. Right panel shows SC encounter with the dust-loaded plume and stagnated ion flow (case B). Times (UT) are labeled at 1-min intervals during close approach on March 12, 2008.

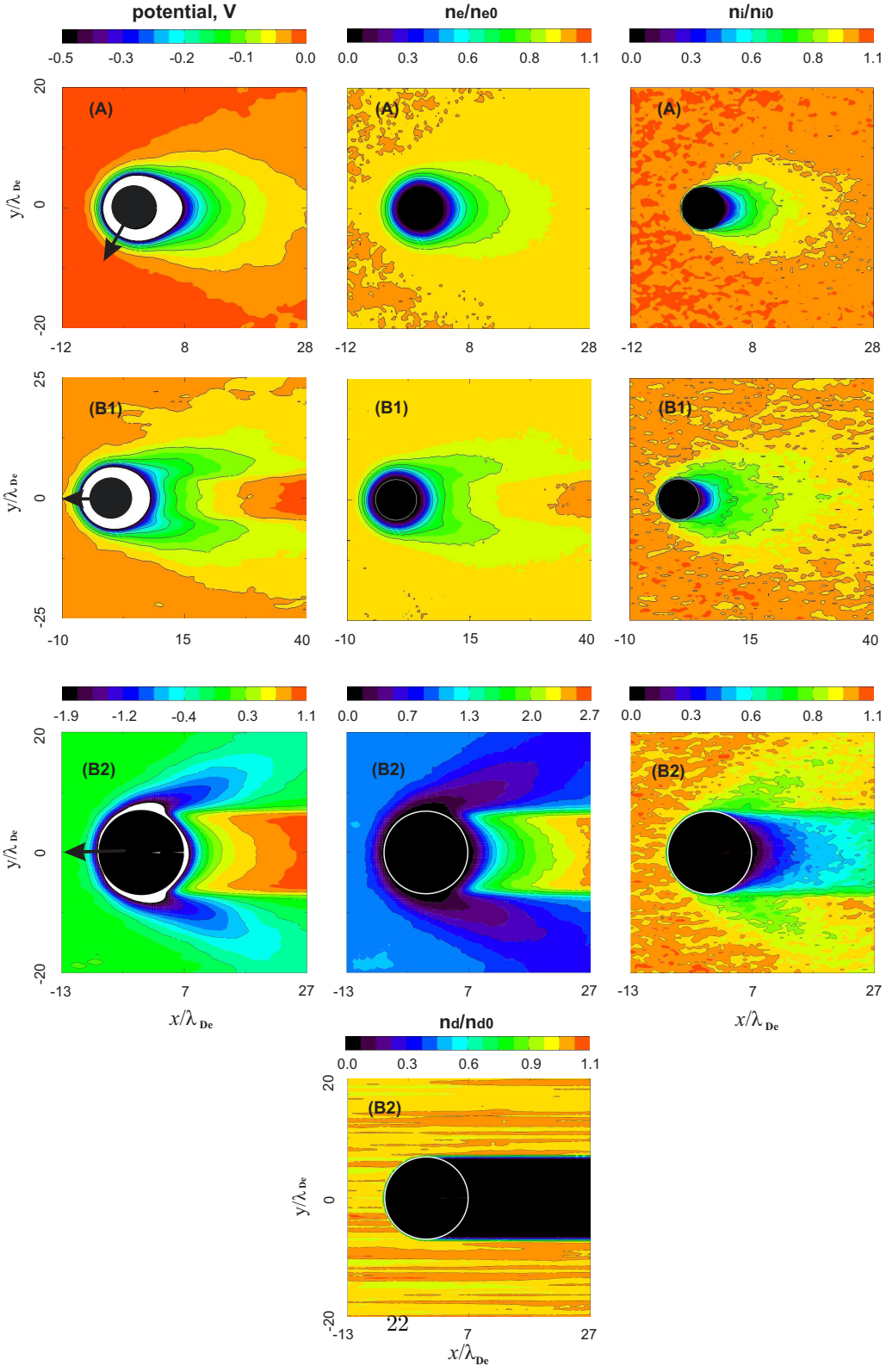

Figure 2: Contour plots of electric potential distribution ψ, normalized electron (n_e/n_{e0}), ion (n_i/n_{i0}) and dust (n_d/n_{d0}) densities in the (xy) plane simulated for the SC positions A (upper panel) and B (panels B1 and B2, respectively), shown in Fig. 1. Length scales are in units of the electron Debye length, $\lambda_D = (4\pi e^2 n_{e0}/m_e)^{1/2}$ which is 0.959 m (A), 0.783 m

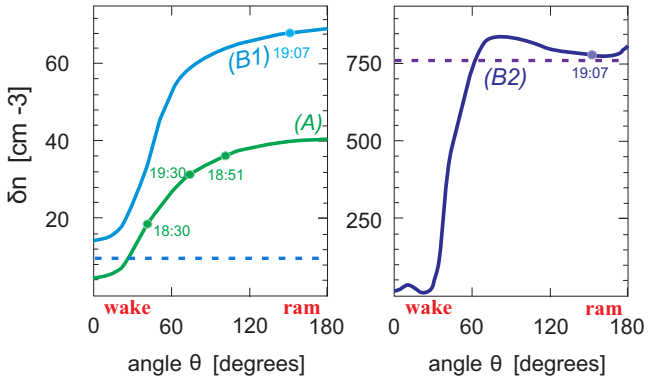

Figure 3: Angular distributions of the plasma imbalance, $\delta n(\theta)$, in the (x, y) plane calculated for a 1.5 m distance from the SC surface which corresponds to $\sim 1.5\lambda_D$ (A) $\sim 2\lambda_D$ (B1) and $\sim 3\lambda_D$ (B2). Left panel shows $\delta n(\theta)$ for A and B1 plasmas; right panel presents $\delta n(\theta)$ in the dust-loaded case, B2. Dashed lines indicate the ambient plasma imbalance for B1 and B2. The actual LP orientations in terms of angle θ are marked for the encounter E3.

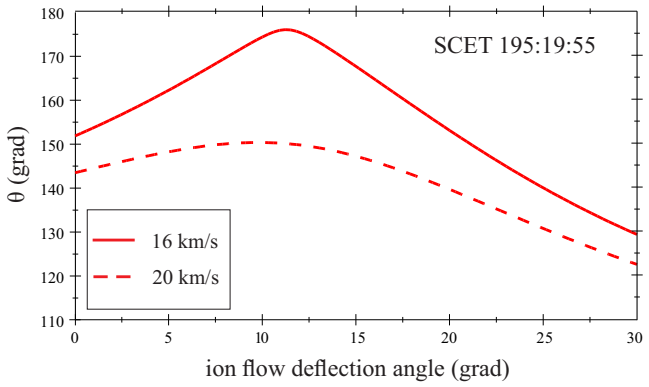

Figure 4: Variations of the LP orientation angle θ due to deflection of the co-rotating flow (angle α counts from athimuthal direction) for ion flow velocities $V_{cor} = 16$ and $V_{cor} = 20$. Calculations are performed using Cassini ephemeris during at SCET195:19:55 h (E2 flyby).